The vertical age profile in sea ice: theory and numerical results

Olivier Lietaer[a,b,*], Eric Deleersnijder[a,c], Thierry Fichefet[c], Martin Vancoppenolle[c], Richard Comblen[d], Sylvain Bouillon[c,a], Vincent Legat[a,b]

[a] Université catholique de Louvain
Institute of Mechanics, Materials and Civil engineering (iMMC)
4, Avenue Georges Lemaître, B-1348 Louvain-la-Neuve, Belgium.

[b] Université catholique de Louvain
Georges Lemaître Centre for Earth and Climate Research (TECLIM)
2, chemin du Cyclotron, B-1348 Louvain-la-Neuve, Belgium.

[c] Université catholique de Louvain
Earth and Life Institute (ELI)
Georges Lemaître Centre for Earth and Climate Research (TECLIM)
2, chemin du Cyclotron, B-1348 Louvain-la-Neuve, Belgium.

[d] e-Xstream engineering
Z.I. Bommelscheuer L-4940 Bascharage, Luxembourg.

Abstract

The sea ice age is an interesting diagnostic tool because it may provide a proxy for the sea ice thickness and is easier to infer from observations than the sea ice thickness. Remote sensing algorithms and modeling approaches proposed in the literature indicate significant methodological uncertainties, leading to different ice age values and physical interpretations. In this work, we focus on the vertical age distribution in sea ice. Based on the age theory developed for marine modeling, we propose a vertically-variable sea ice age definition which gives a measure of the time elapsed since the accretion of the ice particle under consideration. An analytical solution is derived from Stefan's law for a horizontally homogeneous ice layer with a periodic ice thickness seasonal cycle. Two numerical methods to solve the age equation are proposed. In the first one, the domain is discretized adaptively in space thanks to Lagrangian particles in order to capture the age profile and its discontinuities. The second one focuses on the mean age of the ice using as few degrees of freedom as possible and is based on an Arbitrary Lagrangian-Eulerian (ALE) spatial discretization and the finite element method. We observe an excellent agreement between the Lagrangian particles and the analytical solution. The mean value and the standard deviation of the finite element solution agree with the analytical solution and a linear approximation is found to represent the age profile the better, the older the ice gets. Both methods are finally applied to a stand-alone thermodynamic sea ice model of the Arctic. Computing the vertically-averaged ice age reduces by a factor of about 2 the simulated ice age compared to the oldest particle of the ice columns. A high correlation is found between the ice thickness and the age of the oldest particle. However, whether or not this will remain valid once ice dynamics is included should be investigated. In addition,

*Corresponding author. E-mail: olivier.lietaer@uclouvain.be, Tel: +32 10 47 23 57, Fax: +32 10 47 21 80

the present study, based on thermodynamics only, does not support a single age-thickness functional relationship.

Keywords: Ice age, age theory, thermodynamic sea ice model, Lagrangian, ALE

1 Introduction

Sea ice age patterns and how they change in time provide an integrated view of the recent evolution of sea ice growth, melt and circulation, and therefore give some information on the recent thinning of Arctic sea ice. The sea ice age may also provide a means to retrieve the ice thickness, as older ice is typically thicker. For these reasons, the age of Arctic sea ice has recently been the subject of several remote sensing and modeling studies (Walsh and Zwally, 1990; Nghiem et al., 2007; Maslanik et al., 2007; Vancoppenolle et al., 2009; Hunke and Bitz, 2009).

Sea ice age inferred from satellite ice concentration and motion data has been used as a proxy for ice thickness because of the difficulties to observe ice thickness from space. Typically, the satellite sea ice age products (Rigor and Wallace, 2004; Fowler et al., 2004; Belchansky et al., 2005) are based on (i) the creation of sea ice with age zero in open water, (ii) horizontal advection of the age using gridded fields of ice motion, (iii) ageing of sea ice with time and (iv) disappearance of ice of any age lying outside the limits of the ice edge. The age evaluated in this manner corresponds to the time elapsed since the creation of an ice parcel and is available at large scales. However, there are significant differences in sea ice age among the different algorithms used. In addition, those algorithms neglect several processes, including the vertical processes of sea ice growth and melt, which could have a significant role.

In order to understand how ice thickness can be inferred from sea ice age, the latter has been introduced in large-scale sea ice models (Vancoppenolle et al., 2009; Hunke and Bitz, 2009). Sea ice age is considered in those models as a two-dimensional tracer, following ice area (Vancoppenolle et al., 2009) or ice volume (Hunke and Bitz, 2009). This implies horizontal transport and redistribution in thickness space due to thermodynamic and mechanical processes. Besides, new ice formed at the base or at the surface is assumed to have the same age as the rest of the column. Thereby, modelers intend to mimic the sea ice age derived from satellite observations which do not consider the role of vertical processes. Using such definitions for sea ice age, model studies found some difficulties to derive ice thickness from ice age. Besides, those studies indicate large methodological uncertainties. For instance, Harder (1997) proposes another approach where new bottom ice is considered as a sink of ice age, and Hunke and Bitz (2009, Fig. 9) show that integrating bottom growth in the ice age induces a decrease in the simulated sea ice age by more than a factor of 2. This illustrates how the choice of the age definition leads to different values and physical interpretations, which is well known in marine modeling (see Deleersnijder et al., 2001).

The ice age vertical profile accounts for subsurface processes that satellite cannot see. Hence, understanding the sea ice age vertical profile provides a theoretical framework for understanding satellite retrievals. Of particular interest is bottom ice growth that reduces the average ice age. The sea ice age vertical profile also tells us about the history of the ice formation, and therefore about recent changes in the thermodynamic evolution of the ice pack in the context of climate change. Furthermore, sea ice age is an interesting diagnostic that is related with several sea ice physical properties: ice strength (Timco and Frederking, 1990; Kovacs, 1997), salinity (Nakawo and Sinha, 1981; Schwarzacher, 1959), surface topography (Eicken et al., 2004).

There are two fundamental questions that are addressed here. First, what are the ranges for sea ice age associated with vertical thermodynamic processes? Second, what is the nature of the relation between ice age and thickness, considering the vertical thermodynamics of sea

ice? To address these questions, we consider a vertically-variable sea ice age, based on the age theory developed for marine modeling by Delhez et al. (1999) and Deleersnijder et al. (2001) [1]. In contrast to previous modeling studies, we define the sea ice age as the time elapsed since the ice particle under consideration has been formed at the ice base and explicitly compute the vertical age profile. Horizontal advection and redistribution in thickness space are not taken into account. We first analyze the one-dimensional problem of vertical variations of sea ice age associated with seasonal growth and melt. The basal growth of sea ice tends to establish a simple increase of ice age with height, while the summer melt introduces a distinct stratification of annual growth layers. The discontinuities in sea ice age between annual layers are particularly difficult to handle numerically. Then we generalize to larger scales in order to understand the broader implications.

Section 2 presents some concepts of the age theory and its application to a simple model of the evolution of an ice layer, yielding an analytical solution for the ice age. Two numerical methods are provided in section 3 to solve the ice age equation and results thereof are analyzed and compared against the analytical solution. These methods are finally applied to a more realistic thermodynamic model of sea ice (section 4) and the paper is closed with discussions on the method and some perspectives.

2 The ice age: concepts and analytical solution

The concepts of the ice age are presented and a general equation of evolution of the ice age is derived in a three-dimensional framework. We will then deduce the ice age equation for different vertical coordinates and in the particular case of a one-dimensional domain. Finally, an analytical solution of the vertical age profile in sea ice is deduced.

2.1 The theory of the age applied to sea ice

Let us first derive the evolution equation for age in sea ice. From a general point of view, the sea ice age can be considered as a three-dimensional tracer. If (x, y, z) denote the cartesian coordinates and t time ($t = 0$ at the beginning of the accretion period), we attach the coordinate system to a given material surface of the ice at time $t = 0$, defining the level of reference $z = 0$ (Fig. 1). The z axis points upwards and the x and y axes are horizontal and define an orthogonal basis. The ice thickness can be defined as:

$$H(x, y, t) = z_s(x, y, t) - z_b(x, y, t),$$

where $z_b(x, y, t)$ and $z_s(x, y, t)$ denote the height (positive upwards) of the bottom and surface of the ice column. These interfaces are time-dependent and define a domain with moving boundaries. The boundaries evolve according to the rate of change in ice thickness (q) which can be decomposed in surface (q_s) and basal (q_b) components:

$$q(x, y, t) = q_s(x, y, t) + q_b(x, y, t). \tag{1}$$

We further assume that the ice is moving in a "solid block" way -that is, the ice velocity does not depend upon the vertical coordinate. Accordingly, in this referential, ice particles are created or removed at the two free surfaces and keep the same height: the vertical velocity is zero (the trajectories of several ice particles are illustrated in Fig. 2). In particular, the Eulerian and Lagrangian kinematical descriptions are thus equivalent in the vertical coordinate. Obviously, this referential is not the physical frame of reference, as the sea ice vertical velocity is not vanishing in the general case. Moreover, Archimedes' force acting differently at each location would induce an additional motion that could create internal stress and deformation in the ice layer.

[1] This theory is a component of CART (Constituent-oriented Age and Residence time Theory, http://www.climate.be/CART).

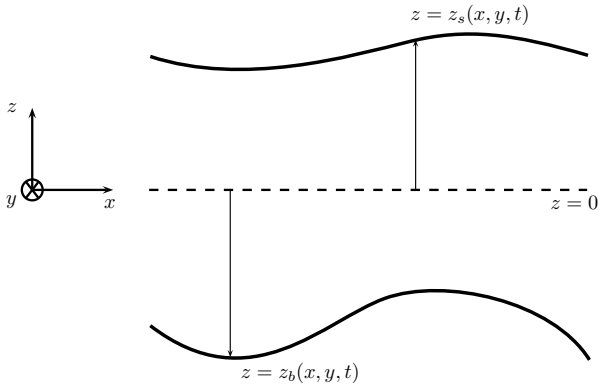

Figure 1: Sketch of the domain $\Omega(t)$. We define the coordinate system as attached to a given material surface of the ice at time $t = 0$. The ice thickness is given by $H(x, y, t) = z_s(x, y, t) - z_b(x, y, t)$.

Following Delhez et al. (1999), the age of a particle of a given continuum is defined as "*the time elapsed since the particle under consideration left the region in which its age is prescribed to be zero*". From a Lagrangian point of view, an ice particle "carries along" its age which increases at the same rate as time passes. In other words, the age of an ice particle is the time elapsed since it was "created". In mathematical terms, the equation for the three-dimensional ice age states that the material derivative of the ice age $a(x, y, z, t)$ must be equal to unity:

$$\frac{Da}{Dt}(x, y, z, t) = 1. \tag{2}$$

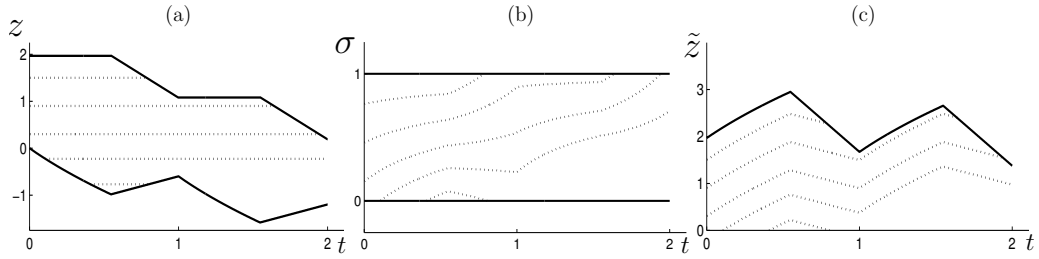

Figure 2: Evolution of the ice thickness in function of time (years) illustrated in the three coordinate systems. In this sketch, ice accretion occurs at the ice bottom and ice ablation at both interfaces. The same particles trajectories in the vertical direction (dotted lines) are illustrated in each domain. (a) Original domain. The level of reference is 0. In this referential, particles have a zero vertical velocity and thus keep the same height. (b) Same, but using the σ coordinates. Using this ALE description, particles are now moving according to the accretion/melting rates at both interfaces, which is expressed by the velocity ω of the particles in the referential domain (see equation (11)). (c) Same, but using the distance to the bottom coordinates ($\tilde{z}$). Particles are moving according to the accretion/melting rates at the ice bottom only, which is expressed by the velocity $\tilde{w}$ of the particles in this domain (see equation (17)).

The general boundary value problem for the ice age $a(x, y, z, t)$ consists in solving equation (2)

$$\frac{\partial a}{\partial t}(x, y, z, t) + u(x, y, t)\frac{\partial a}{\partial x}(x, y, z, t) + v(x, y, t)\frac{\partial a}{\partial y}(x, y, z, t) \quad = \quad 1, \tag{3}$$

on the unknown moving domain

$$\Omega(t) = \{(x, y, z) \in R^3 \text{ such that } z_b(x, y, t) \leq z \leq z_s(x, y, t)\}. \tag{4}$$

We denote by (u, v) the horizontal components of the ice velocity. In terms of boundary conditions, we impose that the age of newly frozen ice is zero. We need to define an initial age field, but its importance is weak: as soon as all the initial ice has melted, the ice age will be correctly defined in the whole ice layer. Equation (3) is hyperbolic, and the ice age must be prescribed where ice is formed:

$$\begin{aligned} a(x,y,z,0) &= a_0(x,y,z), && (5)\\ a(x,y,z_b,t) &= 0, \quad \text{if } q_b(x,y,t) > 0, && (6)\\ a(x,y,z_s,t) &= 0, \quad \text{if } q_s(x,y,t) > 0. && (7) \end{aligned}$$

The motion of the ice bottom and surface are prescribed by the thermodynamic rates of change in ice thickness:

$$\begin{aligned} \frac{\partial z_b}{\partial t}(x,y,t) + u(x,y,t)\frac{\partial z_b}{\partial x}(x,y,t) + v(x,y,t)\frac{\partial z_b}{\partial y}(x,y,t) &= -q_b(x,y,t), && (8)\\ \frac{\partial z_s}{\partial t}(x,y,t) + u(x,y,t)\frac{\partial z_s}{\partial x}(x,y,t) + v(x,y,t)\frac{\partial z_s}{\partial y}(x,y,t) &= q_s(x,y,t). && (9) \end{aligned}$$

Note that the boundary condition (7) covers the case where ice is formed at the surface, so that the boundary value problem (3)-(9) is general.

In order to transform the problem from a moving domain to a fixed reference domain, we introduce the following change of variable for the vertical coordinate:

$$\sigma(x,y,z,t) = \frac{z - z_b(x,y,t)}{z_s(x,y,t) - z_b(x,y,t)},$$

defining a new referential which has the advantage of keeping the height of the domain constant. Actually, these coordinates define an Arbitrary Lagrangian-Eulerian (ALE) formalism (e.g., Donea et al., 2004). In the ALE description, the computational grid is neither fixed in space, nor associated with material points. In this formalism, the ice bottom is mapped onto $\sigma = 0$ and the surface onto $\sigma = 1$. Note that this coordinate is similar to the sigma coordinate defined in ocean modeling (Phillips, 1957). In the equation for the age, a vertical velocity ω has to be introduced in order to take into account the motion in the domain:

$$\frac{\partial a}{\partial t}(x,y,\sigma,t) + u(x,y,t)\frac{\partial a}{\partial x}(x,y,\sigma,t) + v(x,y,t)\frac{\partial a}{\partial y}(x,y,\sigma,t) + \omega(x,y,\sigma,t)\frac{\partial a}{\partial \sigma}(x,y,\sigma,t) = 1. \quad (10)$$

The particle velocity ω can be directly obtained as a linear combination of the rates of change in ice thickness at the ice bottom and surface (Fig. 2b):

$$\omega(x,y,\sigma,t) = \frac{(1-\sigma)\, q_b(x,y,t) - \sigma q_s(x,y,t)}{z_s(x,y,t) - z_b(x,y,t)}. \quad (11)$$

The initial and boundary conditions associated to equation (10) are:

$$\begin{aligned} a(x,y,\sigma,0) &= a_0(x,y,\sigma), && (12)\\ a(x,y,0,t) &= 0, \quad \text{if } q_b(x,y,t) > 0, && (13)\\ a(x,y,1,t) &= 0, \quad \text{if } q_s(x,y,t) > 0. && (14) \end{aligned}$$

For notational convenience, we also define a local vertical coordinate by:

$$\tilde{z}(x,y,z,t) = z - z_b(x,y,t), \quad (15)$$

which refers to the distance to the ice bottom (Fig. 2c). This transformation belongs again to an ALE formalism and equation (2) becomes:

$$\frac{\partial a}{\partial t}(x,y,\tilde{z},t) + u(x,y,t)\frac{\partial a}{\partial x}(x,y,\tilde{z},t) + v(x,y,t)\frac{\partial a}{\partial y}(x,y,\tilde{z},t) + \tilde{w}(x,y,t)\frac{\partial a}{\partial \tilde{z}}(x,y,\tilde{z},t) = 1, \quad (16)$$

where

$$\tilde{w}(x, y, t) = q_b(x, y, t), \tag{17}$$

corresponding to the intuition that the distance separating a material point from the bottom of the ice is only dictated by the ice growth/melt at the ice bottom. Accordingly, in absence of ice accretion or melting at the bottom, an ice particle keeps the same relative height in the ice. The converted initial and boundary conditions to close the problem are:

$$a(x, y, \tilde{z}, 0) = a_0(x, y, \tilde{z}), \tag{18}$$

$$a(x, y, 0, t) = 0, \quad \text{if } q_b(x, y, t) > 0, \tag{19}$$

$$a(x, y, z_s - z_b, t) = 0, \quad \text{if } q_s(x, y, t) > 0. \tag{20}$$

2.2 A simple model of sea ice accretion and melting

In the remainder of this paper, we will focus on the vertical profile of the ice age, neglecting the horizontal advection. Changes in the surface energy budget shape the seasonal cycle of ice thickness. In this section, an analytical model of sea ice growth and melt forced by changes in air temperature is introduced. The model combines the classical model of Stefan (1891) for sea ice growth and a linear parameterization of melt. This model is able to reproduce the salient features of sea ice growth and melt. However, being highly idealized, it is not meant to provide accurate simulations of ice thickness.

2.2.1 Stefan's law

Assume that the ice layer under study is horizontally homogeneous and infinite, implying that only vertical heat fluxes are to be taken into account. During the accretion period, we assume that only ice accretion occurs at the bottom of the ice. If $F_C(t)$ denotes the conductive heat flux (the fluxes directed to the ice surface are taken to be positive) and if we neglect the oceanic heat flux, the growth rate of $H(t)$, the ice thickness, satisfies the following expression:

$$L\frac{dH}{dt} = F_C, \tag{21}$$

where L represents the volumetric latent heat of fusion of ice (see Table 1).

Parameter	Symbol	Value	Unit
Volumetric latent heat of fusion	L	3×10^8	J m^{-3}
Thermal conductivity	k	2.1	W m^{-1} °C^{-1}
1 year	T	365×86400	s
Duration of accretion season	T_a	200×86400	s
Duration of melting season	T_m	165×86400	s
Bottom temp. - top temp.	$\Delta\theta$	20	°C
Conductive heat flux	F_C	parameterized	W m^{-2}

Table 1: Table with principal parameters and values used for the simple model of ice accretion and melting.

At the lower boundary of the ice, the ice temperature is that of the melting point. At the upper boundary, the air temperature largely influences the ice temperature. The difference, $\Delta\theta$, between the temperatures of the ice bottom and the ice surface is positive during the accretion season, and is considered a constant in the present approach. By neglecting thermal inertia and internal heat sources, the temperature difference $\Delta\theta$ is associated with a heat flux, which, in Stefan's model, is assumed to be constant over the height of the ice. Therefore, according to Fourier's law, the upward conductive heat flux F_C taking place in the ice may be parameterized

as $k\Delta\theta/H$, where k is the thermal conductivity of ice (Table 1). The differential equation that the ice thickness must satisfy during the accretion period is:

$$H\frac{dH}{dt} = k\frac{\Delta\theta}{L}. \tag{22}$$

Without any loss of generality, the ice accretion period may be assumed to start at time $t = 0$. If $H_0 = H(0)$ and if T_a is the duration of the accretion period, then the ice thickness grows as

$$H(t) = \sqrt{H_0^2 + \alpha t}\,, \quad 0 \le t \le T_a, \tag{23}$$

where α depends on various physical parameters (see Table 1):

$$\alpha = \frac{2k\Delta\theta}{L}. \tag{24}$$

Then, the ice thickness at the end of the cold season reads:

$$H_1 = \sqrt{H_0^2 + \alpha T_a}. \tag{25}$$

2.2.2 The melting period and the periodic regime

During the warm season, we assume that only the upper part of the ice melts, and, for simplicity, that the melting rate is constant. It is now further assumed that the ice layer evolution exhibits a periodic regime (Fig. 3.) with a period of one year, implying that the ice thickness at the beginning of the accretion period (H_0) must be equal to that attained at the end of the warm season (H_2). The periodicity of the ice thickness seasonal cycle allows us to compute the ice height ΔH frozen and melted each year:

$$\Delta H = H(T_a) - H_0 = \sqrt{H_0^2 + \alpha T_a} - H_0. \tag{26}$$

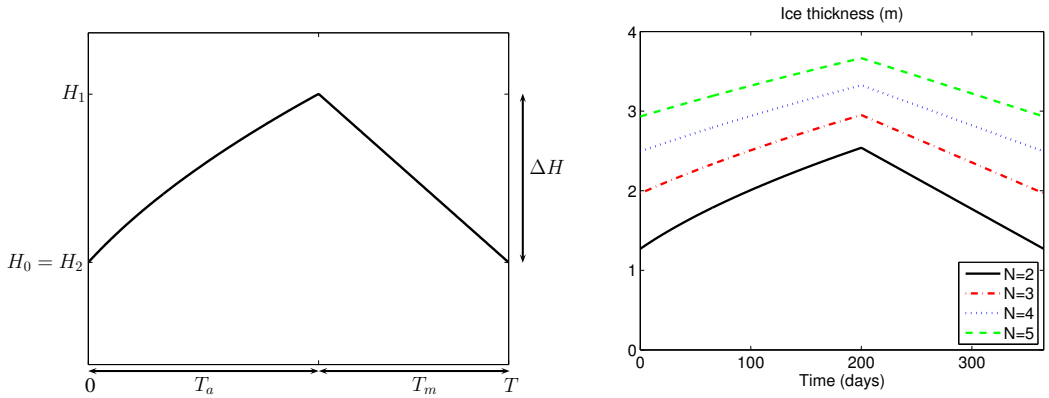

Figure 3: Left: periodic regime of the ice thickness ($H_2 = H_0$); ΔH denotes the ice height frozen and melted each year. Right: ice thickness seasonal cycles obtained for the parameters described in Table 1 and for various values of N (integer relating the maximum ice thickness to ΔH).

Taking the hypothesis of the constant melting rate into account, the ice thickness evolves according to:

$$H(t) = \begin{cases} \sqrt{H_0^2 + \alpha t}, & 0 \le t \le T_a \\ \sqrt{H_0^2 + \alpha T_a} - \frac{t - T_a}{T_m}\Delta H, & T_a \le t \le T_a + T_m \end{cases} \tag{27}$$

where T_m is the duration of the melting period and ΔH is given by equation (26). If we further consider that the maximum ice thickness is an integer multiple (N) of the ice height ΔH frozen and melted each year (see Fig. 3):

$$H_0 + \Delta H = N\Delta H, \tag{28}$$

we can derive an analytical expression for H_0:

$$H_0 = \sqrt{\frac{(N-1)^2 \alpha T_a}{2N-1}}. \tag{29}$$

2.3 An analytical solution of the ice age for the periodic regime

In order to determine an analytical solution for the vertical profile of the sea ice age, we will consider the following hypotheses: (i) the ice layer is horizontally homogeneous, (ii) horizontal advection is neglected, (iii) the ice thickness seasonal cycle is split into two non overlapping periods (growth and melt), (iv) the simple thermodynamic model of Stefan (1891) is used to compute the ice growth, (v) the ice thickness decreases linearly during the melting period, (vi) a periodic regime of the ice thickness seasonal cycle is considered and (vii) the maximum ice thickness is an integer multiple (N) of the ice height ΔH frozen and melted each year.

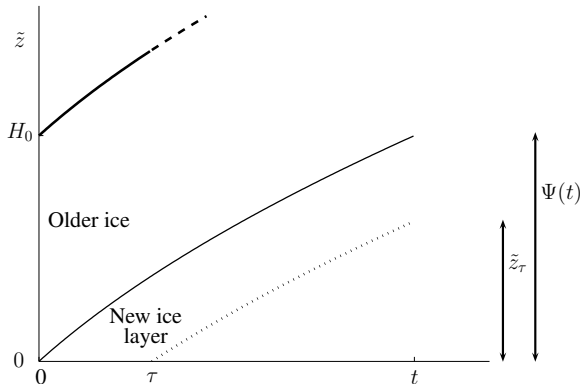

Figure 4: Sketch of the evolution of the newly formed ice layer. H_0 denotes the ice thickness at the beginning of the accretion period ($t = 0$). $\Psi(t)$ represents the ice thickness accumulated since the beginning of the ice accretion period. $\tilde{z}_\tau(t)$ is the distance to the ice bottom at time t of the particle formed at time τ.

The first step of the derivation of the analytical solution focusses on the newly formed ice layer (see Fig. 4). We first consider the ice accretion period. Let $\Psi(t)$ denote the total ice growth since the beginning of the growth season ($t = 0$):

$$\Psi(t) = H(t) - H_0 = \sqrt{H_0^2 + \alpha t} - H_0. \tag{30}$$

We naturally have the following requirements for the ice age of the newly formed ice:

$$0 \leq t \leq T_a, \tag{31}$$
$$0 \leq \tilde{z} \leq \Psi(t), \tag{32}$$
$$a(0,t) = 0, \tag{33}$$
$$a(\Psi(t),t) = t, \tag{34}$$
$$0 \leq a(\tilde{z},t) \leq t, \tag{35}$$

which state that the ice age is greater than zero (for newly formed ice) and smaller than t (for ice frozen at the beginning of the accretion period). In one dimension, equation (16) reads:

$$\frac{\partial a}{\partial t}(\tilde{z},t) + q_b(t)\frac{\partial a}{\partial \tilde{z}}(\tilde{z},t) = 1. \tag{36}$$

An elegant way of solving the ice age equation (36) is to consider the growth of the ice layer as a streakline, i.e. a geometrical curve generated by the continuous emission of particles from a given position in space (here $\tilde{z} = 0$). The streakline is described at the time t as the ensemble of particles of Lagrangian coordinate z such that at a given time τ we have $\tilde{z}(z, \tau) = 0$. Its parametric equation is given by:

$$\tilde{z}_\tau = \tilde{z}(z(0, \tau), t), \qquad 0 \leq \tau \leq t \tag{37}$$

where $z = z(\tilde{z}, t)$ is the inverse one-to-one mapping from the referential to the original domain. Following equation (17), the parametric equation of the streakline is the solution of the following differential expression:

$$\frac{\partial \tilde{z}_\tau}{\partial t} = q_b(t), \tag{38}$$

and, according to hypothesis (iii), $q_b(t) = \frac{dH(t)}{dt}$ here. Equation (38) gives then by integration between τ and t:

$$\tilde{z}_\tau = \sqrt{H_0^2 + \alpha t} - \sqrt{H_0^2 + \alpha \tau}, \tag{39}$$

thanks to equation (23). In a Lagrangian framework, the age of this particle must satisfy equation (3):

$$\frac{\partial a}{\partial t}(z(0, \tau), t) = 1, \tag{40}$$

with $a(z(0, \tau), \tau) = 0$, yielding by integration again:

$$a(z(0, \tau), t) = t - \tau = a(\tilde{z}_\tau, t). \tag{41}$$

Equation (39) can be rearranged as (dropping the subscript τ):

$$\tau = t - \frac{2\tilde{z}}{\alpha}\sqrt{H_0^2 + \alpha t} + \frac{\tilde{z}^2}{\alpha}, \qquad 0 \leq \tilde{z} \leq \Psi(t). \tag{42}$$

Substituting equation (42) in equation (41), the age of the newly formed ice is finally given by:

$$a(\tilde{z}, t) = \frac{2\tilde{z}}{\alpha}\sqrt{H_0^2 + \alpha t} - \frac{\tilde{z}^2}{\alpha}, \qquad 0 \leq \tilde{z} \leq \Psi(t). \tag{43}$$

Using equation (43), we now can get the age in the newly formed ice layer during the whole year:

$$a^{new}(\tilde{z}, t) = \begin{cases} \frac{2\tilde{z}}{\alpha}\sqrt{H_0^2 + \alpha t} - \frac{\tilde{z}^2}{\alpha}, & 0 \leq t \leq T_a \\ \frac{2\tilde{z}}{\alpha}\sqrt{H_0^2 + \alpha T_a} - \frac{\tilde{z}^2}{\alpha} + t - T_a, & T_a \leq t \leq T_a + T_m \end{cases}$$

Finally, for the remainder of the ice column, we introduce the integer i to determine in which annual layer we are:

$$i = \left\lfloor \frac{\tilde{z} - \Psi(t)}{\Delta H} \right\rfloor \tag{44}$$

where $\lfloor x \rfloor$ is the largest integer smaller than or equal to x. The first annual layer is characterized by $i = 0$, and its age is comprised between t and $t + 1$ year, etc. We can now finally generalize the ice age for the whole column:

$$a(\tilde{z}, t) = \begin{cases} a^{new}(\tilde{z}, t), & 0 \leq \tilde{z} \leq \Psi(t) \\ a^{new}(\tilde{z} - \Psi(t) - i\Delta H, T) + t + iT, & \Psi(t) \leq \tilde{z} \leq H(t), \end{cases}$$

where $T = 1$ year.

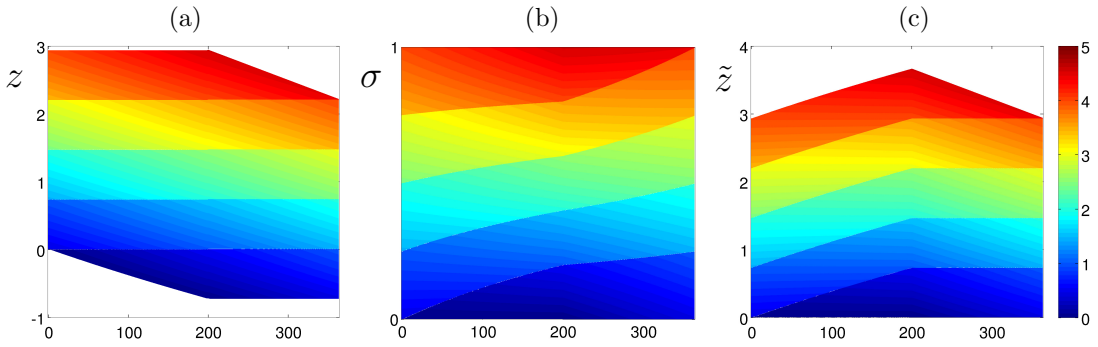

Figure 5: (a) Time series (in days) of the analytical sea ice age ($N = 5$, 0-5 years) contoured in the sea ice domain. (b) Same, but in the σ domain. (c) Same, but in the $\tilde{z}$ domain. As expected, the age gets older with height. The sharp variations in colour between two growth seasons illustrate the annual stratification of the ice column and the discontinuities in the age profile.

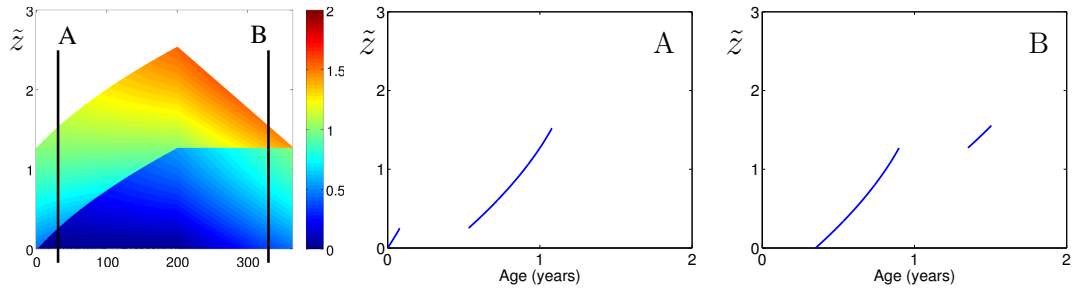

Figure 6: Left: time series (in days) of the analytical sea ice age ($N = 2$, 0-2 years) contoured in the $\tilde{z}$ domain. Centre: profile A (snapshot after 1 month) of sea ice age. Right: profile B (after 11 months). The discontinuity in ice age corresponds to the duration of the melt season.

The analytical solution is illustrated in figures 5 and 6. Fig. 5 shows the time series (in days) of the analytical sea ice age contoured in the sea ice domain for the three different coordinates (case $N = 5$). The periodicity of the ice regime is obvious. In the z domain (Fig. 5a), the reference level is taken to be the ice bottom at the beginning of the accretion period. In this simple model, ice particles are formed at the ice bottom during the accretion period and keep the same height until they melt at the ice surface during the melting period. The age thus gets older with height and is comprised between 0 and 5 years. The sharp variations in colour between two growth seasons illustrate the annual stratification of the ice column and the discontinuities in the age profile. Note that the number of annual growth layers corresponds to N and the number of age discontinuities to $N - 1$. When the ice column is described in function of the distance to the bottom (panel (c)), accretion at the ice bottom generates a vertical velocity (see equation (17)), while during summer, we have the same age contour as in the previous referential due to the absence of basal melting. Panel (b) illustrates the same configuration, but using σ coordinates. The fact that the domain is fixed is counterbalanced by a much more complex particles movement depending on the accretion/melting rates at both interfaces (see equation (11)). Fig. 6 illustrates two ice age profiles in the $\tilde{z}$ domain. Profile A corresponds to the growth period. New particles of age 0 are accreted at the ice bottom and the discontinuity in ice age corresponds to the duration of the melt season. Profile B illustrates the melt season. Particles at the ice surface are melted, while the rest of the particles see their age increasing at the same rate as time passes.

3 Numerical methods

We present two numerical methods for solving the sea ice age equation. The first method is designed to capture the vertical profile of sea ice age and its discontinuities. This method can be viewed as a Lagrangian method because the vertical velocity vanishes in our model. Therefore, the Eulerian grid nodes correspond to Lagrangian particles. The second one is based on a finite element method, is computationally cheaper and aims at simulating the mean and standard deviation of the age only. Indeed, the first two usual moments in statistics provide us an overview of the distribution and the mean value corresponds to the volume-averaged ice age. To illustrate both methods' respective strengths and weaknesses, we compare them to the analytical solution.

3.1 Spatial adaptive discretization

We present a simple adaptive approach to compute the vertical profile of the ice age. It consists in updating the age of a large number of ice particles. The vertical resolution can be chosen arbitrarily, the point here being not to enhance the precision but merely the "picture" of the vertical distribution of the ice age that we get. Actually, such a method consists in integrating a partial differential equation along the characteristic and will provide an exact solution if the temporal discretization is performed exactly. This is particularly helpful in a realistic simulation where no analytical solution exists. Since particles only move vertically in this work, the variables in this method are the number n of particles and the distance of the first particle to the bottom (z_0). Also of use are the distance of the last particle to the surface (z_n), the ice thickness (H) and the growth/melt rates. The method is illustrated in Fig. 7.

The particles are updated at each time step in function of the basal and surface growth/melt rates. For the sake of generality, in the sketch of the method (Fig. 7), summer melt has bottom and surface contributions, whereas the analytical solution involves surface melt only. If the distance z_0 (z_n) is larger than the prescribed vertical resolution Δz, we add a particle at the bottom (surface) of the ice layer. If the distance to the bottom (surface) is negative, we remove the first (last) particle. In practice, we store the accretion time of the particles instead of their age, avoiding any further time update. The computational overhead to handle the Lagrangian particles is almost negligible, unlike the memory footprint of this method.

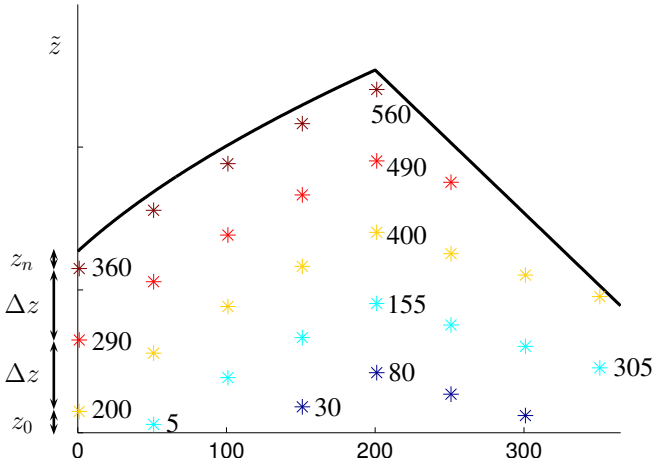

Figure 7: Ice thickness seasonal cycle illustrating the Lagrangian particles method used in this work. z_0 and z_n are the distance of the first particle to the bottom and the distance of the last particle to the surface, respectively, and Δz denotes the vertical resolution. The age of some particles is noted (in days). In this illustration, summer melt has bottom and surface contributions. Bottom melt is responsible for downward motion of the particles in this referential.

3.2 Spatial ALE discretization

The aim of this method is to reproduce the mean and standard deviation of the vertical distribution of the ice age using as few degrees of freedom as possible. The problem is easier to solve numerically on a fixed domain, using the σ coordinates. The boundary value problem (see equations (10)-(14)) that needs to be solved for the vertical ice age profile $a(\sigma, t)$ is summarized as follows:

$$\frac{\partial a}{\partial t}(\sigma, t) + \frac{(1-\sigma)q_b(t) - \sigma q_s(t)}{z_s(t) - z_b(t)} \frac{\partial a}{\partial \sigma}(\sigma, t) = 1, \tag{45}$$

with the following boundary conditions:

$$a(\sigma, 0) = a_0(\sigma), \tag{46}$$

$$a(0, t) = 0, \quad \text{if } q_b(t) > 0, \tag{47}$$

$$a(1, t) = 0, \quad \text{if } q_s(t) > 0, \tag{48}$$

where $q_b(t)$ and $q_s(t)$ are prescribed by the ice thermodynamics. In order to compute the age profile by the finite element method, a variational formulation of this problem must be obtained. To this end, we first multiply equation (45) by a test function $\hat{a}$ and we integrate the partial differential equation over the height of the domain:

$$\frac{d}{dt} \int_0^1 a\hat{a} \mathrm{d}\sigma = -[\omega a \hat{a}]_0^1 + \int_0^1 \left(\frac{\partial (\omega \hat{a})}{\partial \sigma} a + \hat{a} \right) \mathrm{d}\sigma, \tag{49}$$

where the second term of equation (45) has been integrated by parts. Furthermore, the unknown field $a(\sigma, t)$ is approximated by piecewise polynomial functions defined as follows:

$$a(\sigma, t) \approx a^h(\sigma, t) = \sum_{j=0}^{p} a_j(t) \phi_j(\sigma) \tag{50}$$

where $\phi_j(\sigma)$ $(j = 0, 1, \ldots, p)$ are the polynomial shape functions and $a_j(t)$ the unknown degrees of freedom. In a usual Galerkin formulation, the shape functions are used as test functions $\hat{a}$. Taking the boundary condition (47)-(48) and the expression for ω into account, the first term of second member of equation (49) now reads:

$$-[\omega a \phi_i]_0^1 = \frac{q_b^- a(0, t)\phi_i(0) + q_s^- a(1, t)\phi_i(1)}{H}, \quad i = 0, 1, \ldots, p \tag{51}$$

where the $-$ superscripts denote the melt rates. Substituting equations (50) and (51) in (49) gives rise to a system of $p+1$ ordinary differential equations and $p+1$ unknowns $a_j(t)$:

$$\sum_{j=0}^{p} \int_0^1 \phi_i(\sigma)\phi_j(\sigma)\mathrm{d}\sigma \frac{da_j}{dt} = \sum_{j=0}^{p} A_{ij}a_j + \int_0^1 \phi_i(\sigma)\mathrm{d}\sigma, \quad i = 0, 1, \ldots, p \tag{52}$$

where $A_{ij} = \frac{q_b^- \phi_i(0)\phi_j(0) + q_s^- \phi_i(1)\phi_j(1)}{H} + \int_0^1 \left(\frac{\partial(\omega\phi_i)}{\partial\sigma}\phi_j \right) \mathrm{d}\sigma$. The system of equations gets even simpler if one decides to opt for orthonormal shape functions, i.e.

$$\int_0^1 \phi_i(\sigma)\phi_j(\sigma)\mathrm{d}\sigma = \delta_{ij}, \tag{53}$$

where δ_{ij} denotes Kronecker's delta, diagonalizing the mass matrix. Such an orthogonal property is provided by the Legendre polynomials P_j, from which we derive the shape functions:

$$\phi_j(\sigma) = \sqrt{2j+1}\, P_j(2\sigma - 1). \tag{54}$$

These polynomials are illustrated in Fig. 8. The system now takes the following form:

$$\frac{da_i}{dt} = \sum_{j=0}^{p} A_{ij}a_j + \delta_{0i}, \quad i = 0, 1, \ldots, p \tag{55}$$

and is easily discretized in time, using in this work the forward Euler scheme for simplicity. The coefficients of the matrix A are given in the appendix A. The question as to whether it is better to use several piecewise polynomials of low order or one polynomial of higher order resorts to the interpolation problematic and is treated in the appendix B. We find that increasing the number of elements does not enhance significantly the approximation and, in the remainder of the study, we will restrict ourselves to polynomials of degree up to three on one element.

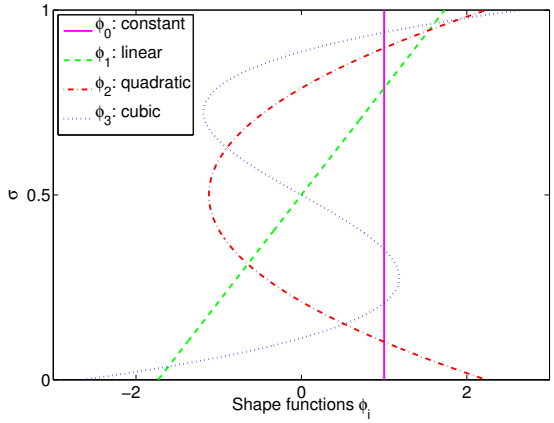

Figure 8: Orthogonal Legendre shape functions used to solve numerically the age equation in function of the normalized vertical coordinate σ.

3.3 Validation with the analytical solution

Numerical results of the Lagrangian particles and the finite element method are compared against the analytical solution derived in section 2. The solutions are shown after a spin-up of 25 years of integration. The vertical resolution of the Lagrangian particles is taken to be $\Delta z = 0.05$ m. For the finite element solutions, we use polynomials of degree up to three on one element.

There is a very good agreement between the analytical solution and the Lagrangian particles (Fig. 9) which are clearly able to reproduce the ice age discontinuities accross melting periods. As one could have expected, the constant finite element approximation clearly is to be rejected. To explain this, we show that the constant approximation corresponds to the mean value $\mu(t)$ of the age distribution:

$$\mu(t) = \int_0^1 a^h(\sigma,t)\mathrm{d}\sigma = \sum_{j=0}^{p} a_j(t) \underbrace{\int_0^1 \phi_j(\sigma)\mathrm{d}\sigma}_{=\delta_{0j}} = a_0(t).$$

In the particular framework of the analytical solution, equation (55) gives the following relationship for the coefficient $a_0(t)$:

$$\frac{da_0(t)}{dt} = \begin{cases} -\frac{q_b(t)}{H(t)}a_0(t) + 1, & 0 \le t \le T_a \\ 1, & T_a \le t \le T_a + T_m. \end{cases} \tag{56}$$

During the accretion period, as the newly frozen ice has an age of zero, the ice growth tends to decrease the mean age ($-\frac{q_b(t)}{H(t)}a_0(t)$ term), counterbalancing the ice ageing process (term equal to 1). During the melting period, the oldest ice is supposed to "melt and carry along its age", decreasing the mean value of the age. However, this effect is not taken into account with a constant age approximation, explaining the (inconsistent) large values of the computed mean age (Fig. 9). In consequence, we will omit the constant approximation for the remainder of this study.

For young ice ($N = 2$, panels a-b), differences between the finite element solutions are clear. In the early accretion period, the cubic approximation gives a negative ice age which has to be rejected. For multiyear ice ($N = 5$, panels c-d), all finite element solutions (except the constant approximation) converge towards a linear evolution of the ice age inside the ice, since no discontinuity is introduced in the solution. This result is similar to the conclusion drawn in appendix B.

In order to determine the accuracy of each method, we compute the root mean square (RMS) error between the numerical approximations and the analytical solution (Table 2). As expected, the Lagrangian particles method shows excellent accuracy to simulate sea ice age and the error is about two orders of magnitude smaller than the error produced by the finite element approximations. As mentioned before, the error is not affected by the number of particles. On the other hand, due to the forward Euler scheme, the error is $O(\Delta t)$ so that, asymptotically, decreasing the time step by two yields an error divided by two. The RMS error of the finite element solutions is approximately the same for any value p. Thus increasing the order of the approximation does not enhance the solution in presence of discontinuities.

N	2	3	4	5	6	7
Lagr.	0.0016	0.0015	0.0017	0.0015	0.0015	0.0015
P_1	0.1326	0.1314	0.1308	0.1305	0.1304	0.1304
P_2	0.1198	0.1253	0.1276	0.1286	0.1291	0.1294
P_3	0.1034	0.1245	0.1281	0.1292	0.1296	0.1298

Table 2: RMS error (in years): Lagrangian particles method (Lagr.) and finite element method: linear (P_1), quadratic (P_2) and cubic (P_3) approximations.

The main goal of the finite element method is to approximate the mean value and standard deviation of the ice age distribution. To evaluate this ability, we compare the mean and standard

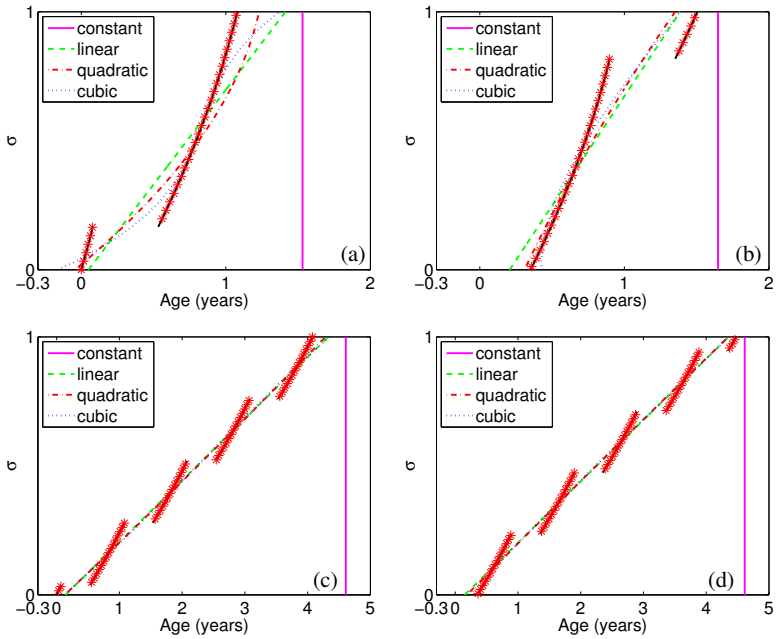

Figure 9: Analytical (solid black line) and numerical solutions of the ice age in function of the normalized vertical coordinate. The red stars represent the Lagrangian particles. The degree of the Legendre polynomials is specified in the legend. (a)-(b) Snapshot of the case $N = 2$ after month 1 (a) and 11 (b). (c)-(d) Same for $N = 5$. Note that each value of the integer N corresponds to an equilibrium state that is reached by the numerical solution after 25 years of integration.

deviation of the analytical solution age distribution with the numerical solution. Based on the finite element method, the standard deviation of the age distribution is computed as:

$$\zeta(t) = \sqrt{\int_0^1 \left[a^h(\sigma,t)\right]^2 \mathrm{d}\sigma - \left[\int_0^1 a^h(\sigma,t)\mathrm{d}\sigma\right]^2} = \sqrt{\int_0^1 \left[\sum_{j=0}^{p} a_j(t)\phi_j(\sigma)\right]^2 \mathrm{d}\sigma - \left[a_0(t)\right]^2}.$$

Thanks to the orthogonality of the shape functions, the standard deviation reads finally:

$$\zeta\left(t\right) = \sqrt{\sum_{j=1}^{p} \left[a_j\left(t\right)\right]^2}.$$

Tables 3 and 4 give the mean and standard deviation of the ice age for the finite element solutions. The linear approximation (P_1) yields satisfactory results which improve for increasing N. Actually, the analytical solution is composed of a linear part with a deviation of mode $N-1$ and of amplitude of the order of half a year. The larger N, the better the linear approximation since the relative importance of the deviation decreases. Again, increasing the order of the finite element approximation does not remarkably enhance the solution.

N	2	3	4	5	6	7
P_1	0.0174	0.0106	0.0071	0.0053	0.0041	0.0032
P_2	0.0229	0.0118	0.0075	0.0055	0.0043	0.0035
P_3	0.0166	0.0095	0.0066	0.0051	0.0041	0.0033
$\bar{\mu}$	0.7634	1.2563	1.7532	2.2512	2.7497	3.2485

Table 3: RMS error of the finite element method on the mean value $\mu(t)$ of the ice age (in years): linear (P_1), quadratic (P_2) and cubic (P_3) approximations. The annual mean of $\mu(t)$ ($\bar{\mu}$) is also shown.

N	2	3	4	5	6	7
P_1	0.0428	0.0246	0.0166	0.0123	0.0094	0.0078
P_2	0.0348	0.0171	0.0111	0.0084	0.0068	0.0058
P_3	0.0246	0.0136	0.0098	0.0078	0.0065	0.0056
$\bar{\zeta}$	0.4247	0.7165	1.0063	1.2956	1.5846	1.8735

Table 4: RMS error of the finite element method on the standard deviation $\zeta(t)$ of the ice age (in years): linear (P_1), quadratic (P_2) and cubic (P_3) approximations. The annual mean of $\zeta(t)$ ($\bar{\zeta}$) is also shown.

4 Application to the large-scale distribution of sea ice age

In this preliminary study, both numerical methods are applied to a stand-alone thermodynamic model of the Arctic sea ice to evaluate the vertical profile of the sea ice age, which, in the case of undeformed ice, is essentially thermodynamically driven. The model used in this study corresponds to the thermodynamic component of the model presented in Lietaer et al. (2008), based on Semtner (1976)'s model. We will restrict ourselves to one category of ice thickness, that is sea ice concentration is kept constant at a value of 1. In the absence of ice transport, the modeled age field gives an approximation of the time needed to thermodynamically grow an ice layer in function of local atmospheric conditions.

4.1 A stand-alone thermodynamic sea ice model of the Arctic

Based on the Semtner (1976) zero-layer thermodynamic scheme, the model neglects the storage of sensible and latent heat, resulting in a linear temperature profile in the ice. Following Fichefet et al. (1998), two boundary conditions are needed, expressed as a heat budget at the surface and at the bottom of the ice. At the upper surface, an equilibrium surface temperature T_s is computed from the heat balance:

$$\underbrace{(1-\alpha)F_r + F_L + F_s + F_l}_{F_A} + F_C = 0, \tag{57}$$

where α is the surface albedo, which in our model is prescribed for each month. F_A is the net atmospheric flux to the upper ice surface and F_C is the conductive flux through ice. Fluxes directed to the ice surface are taken to be positive. In order to solve the heat balance equation, the model includes a parameterization of the solar radiation F_r (Zillmann, 1972), the net longwave radiation F_L (Berliand and Berliand, 1952) and turbulent fluxes of sensible (F_s) and latent (F_l) heat (bulk aerodynamic formulas, see Goosse (1997)). If the predicted T_s is above the melting point T_f, its value is fixed to T_f and the excess of energy is used to melt ice.

At the ice base, temperature is kept at the freezing point of seawater. The melt or growth rate of the ice depends only on the imbalance between the conductive heat flux F_C and the oceanic heat flux F_b:

$$L\frac{dH}{dt} = F_C - F_b, \tag{58}$$

where L represents the volumetric latent heat of fusion of ice. We use a simple slab ocean model and assume that the ocean has a constant mixed layer depth of 30 m. This ocean layer is characterized by a unique temperature that is equal to the freezing point of seawater if there is ice on the area element. When the area element is ice-free, the ocean temperature is computed thanks to a prognostic equation including a heat budget of the oceanic area. The oceanic heat flux is proportional to the difference between the ocean temperature and a climatological temperature of the mixed layer taken from the Polar science center Hydrographic Climatology (PHC 3.0, updated from: Steele et al. (2001)).

Finally, the atmospheric forcing data sets used to run the model are daily NCEP/NCAR reanalysis data for the air temperature and the wind velocity, and monthly climatologies for the relative humidity (Trenberth et al., 1989) and the total cloudiness (Berliand and Strokina, 1980). No snow precipitation is included in the model.

The model here is purely thermodynamic, neglects new ice growth in leads as well as ice transport and deformation. Consequently, ice production and piling are underestimated and the simulated ice thickness gradient between Siberia and Canada is too weak (Fig. 10). However, despite the absence of ice dynamics, ice thickness of up to 6 m is produced along the Canadian Arctic Archipelago and Greenland, which is in agreement with observations (e.g., Bourke and Garrett, 1987; Haas et al., 2010). The presence of very thick ice is the signature of the (low) observed air temperatures used to force the model there. The reanalyses of air temperature are naturally influenced by the cold winds around Greenland and other glaciers and by the very thick ice present along the Canadian Arctic Archipelago. In consequence, the thermodynamic sea ice model reproduces very thick ice in turn. Despite being simple, the model does reasonably simulate the features of Arctic sea ice thickness that are required to understand the thermodynamic controls on the vertical profile of sea ice age.

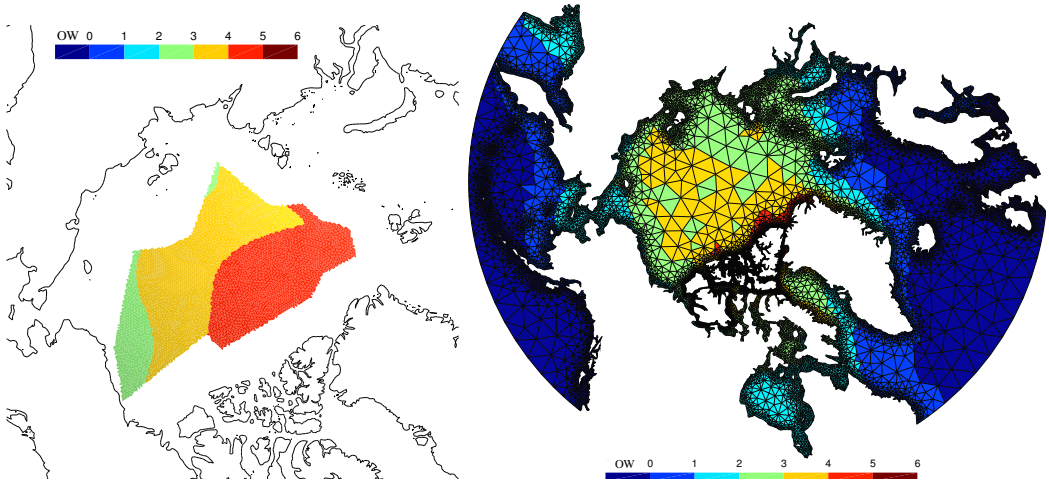

Figure 10: Left: ice thickness climatology from Rothrock et al. (2008) converted from ice draft data collected by naval submarines (April 1975-2000, 0-6 m). Right: global sea ice thickness pattern as computed by the thermodynamic model (April 1979-2000, 0-6 m). OW stands for "open water".

4.2 Results of the large-scale distribution of Arctic sea ice age

The thermodynamic model is spun up for 12 years (so that the initial state of the ice age has vanished) and is then integrated with daily wind and air temperature forcings between 1979 and 2009. The computational domain is situated north of the parallel 50 degrees North and englobes most of the Arctic sea ice. It is composed of triangular elements at the barycenter of which we compute the ice age, following the two methods exposed before. In absence of ice dynamics, everything happens as if each element corresponds to an ice column. In this section, the vertical resolution of the Lagrangian particles is set to $\Delta z = 0.1$ m.

First, a general overview of the maximum age of the ice columns is presented in Fig. 11, based on the Lagrangian particles method. We compute the 1979-2009 March mean age of the oldest Lagrangian particle of each ice column. Within our general framework and hypotheses, in this numerical simulation, most of the sea ice of the Arctic Basin is second- or third-year ice. Due to the influence of Greenland on the air temperature reanalyses, the ice along the coast of Greenland and the Eastern Canadian Arctic Archipelago is thick and old (older than 6

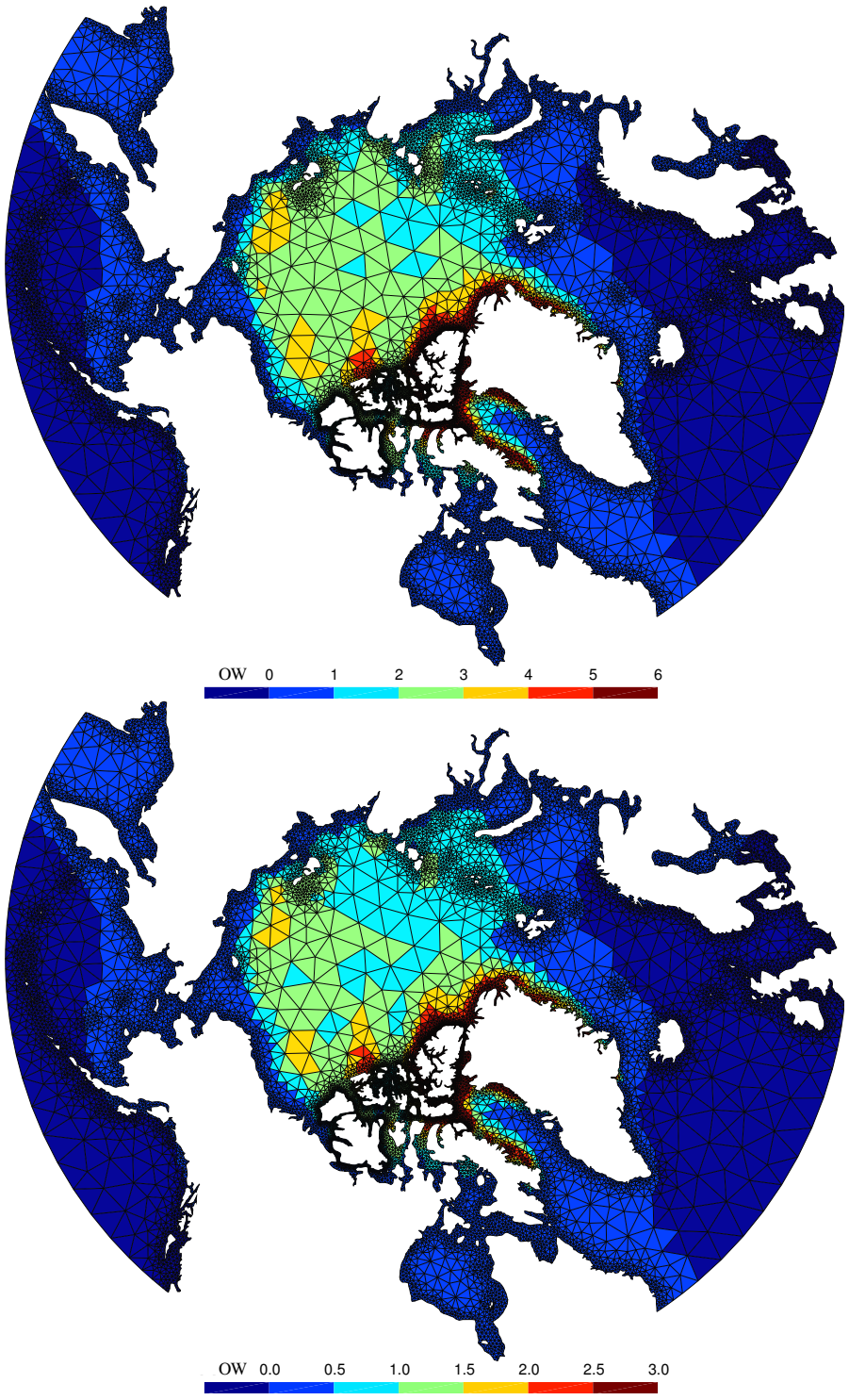

Figure 11: Ice age (March 1979-2009) computed north of the parallel 50 degrees North. Top panel: for each triangular element of this numerical simulation, the long-term mean of the age of the oldest Lagrangian particle is represented. Bottom: same, but the average age of all Lagrangian particles on each vertical profile is shown instead of the age of the oldest particle. Note the different scale. OW stands for "open water".

years). In absence of dynamics, the first-year ice (comprised between 0 and 1 year) matches, by definition, the seasonal ice zone.

The bottom panel of Fig. 11 corresponds to the same result as the top panel, except that the average age of all Lagrangian particles on each vertical profile is shown instead of the age of the oldest particle. This illustrates the two different approaches discussed in the introduction: tracking the surface ice age or allowing bottom ice growth to decrease the ice age, i.e. a volume-averaged ice age. Compared to the top panel, the spatial pattern of sea ice age is very similar, except that the color scale has been divided by two. This factor of approximately two confirms the discrepancy between the two approaches noted by Hunke and Bitz (2009).

At first glance, the correlation between ice thickness (Fig. 10) and the age of the oldest ice particle (Fig. 11, top) seems evident (e.g., most of the first-year ice is smaller than 2 m). Indeed, the overall correlation amounts about 0.84 for the average month of March 1979-2009. However, this correlation is not uniform over the Arctic Basin as shown in Fig. 12. In particular, the correlation is highest in the Beaufort sector (0.97) and lowest in the Kara sector (0.71). It should be noted that, judged from the upper and lower bounds of each year distribution, the scatter follows the typical curve of purely thermodynamically growing ice, i.e. decreasing growth rates with increasing ice thickness and growth towards an equilibrium ice thickness. Therefore, a linear regression fit should not match perfectly by definition. Maslanik et al. (2007) have produced a proxy ice thickness record based on satellite-derived estimates of sea-ice age and thickness. To compare our results, we compute the mean ice thickness for each age class for the same period as Maslanik et al. (2007), i.e. March 2003-2006 (Fig. 13). The model reasonably reproduces the observed ice thickness when considering the observational variance and the large ranges of the modeled ice thicknesses within each ice class. We obtain a strong relationship between mean ice age and mean ice thickness (0.87 for all classes and 0.95 for 1-8 years). However, only the first ice class preserves a high correlation (0.77) when computing the correlation within a single ice class. In our model, the relationship is the image of the growth/melt rates and is thereby subject to the atmospheric variability. Our results are in agreement with Hunke and Bitz (2009): outputs from numerical models show that sea ice age is a good proxy for sea ice thickness when averaged over large spatial and time scales, while the correlation breaks down at smaller scales.

An overview of the evolution of sea ice age is shown in Fig. 14. We compare two different years to illustrate the thermodynamical evolution of the ice near the Canadian Archipelago in our simulation. In this case, we observe ice thinning in the model between 1979-1980 and 2008-2009. This decrease of about 1.5 m corresponds to the signature of the global warming in the air temperature data used to force the model. As can be seen in Fig. 14, the ice column essentially undergoes surface melting, so the ice thinning is coupled to a decrease in sea ice age of about 2 years.

Finally, a couple of snapshots of Arctic ice age profiles are provided in Fig. 15. The right figure illustrates the vertical age profile for the same place as in Fig. 14 for March 2009. The finite element solutions converge towards a linear age profile, missing the age discontinuities between annual layers revealed by the Lagrangian particles method. The ice column surface is almost 7 years old. The centre panel shows a snapshot of second-year ice in Beaufort Sea. Differences between the finite element solutions are clearly marked. The quadratic solution inconsistently predicts a younger ice inside the ice column than at the bottom of it. However, it must be stressed that this method has been designed to compute the mean and standard deviation of the age distribution. For both snapshots, the error in mean age computed by the finite element solutions compared to the particles method is smaller than 10 days and the error in standard deviation does not exceed 13 days. Moreover, the finite element solutions give an approximation of the maximum age of the column (that is, the age at the surface in absence of ice formation at the surface) that is reasonable, considering that sea ice is traditionally classified

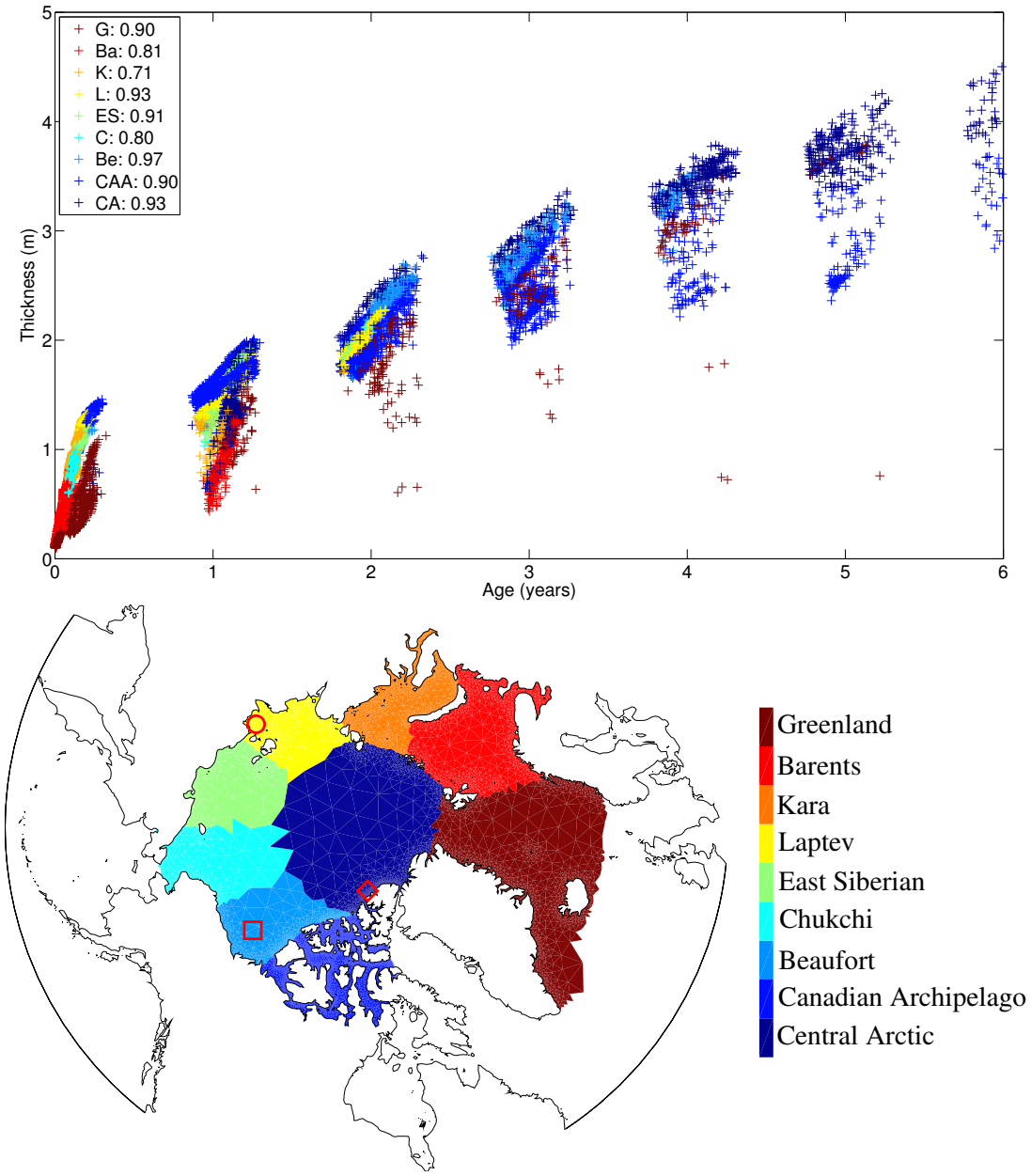

Figure 12: Ice age of the oldest particle at the end of the simulation for each column belonging to one of the sectors described in the bottom figure. The correlation of each sector between the ice age and the ice thickness is mentioned in the legend of the top figure. The melting period induces gaps between crosses clusters that clearly identify ice types (first-year, second-year, ...). Note that for the sake of readability, the top figure has been cropped to ice particles of maximum 6 years.

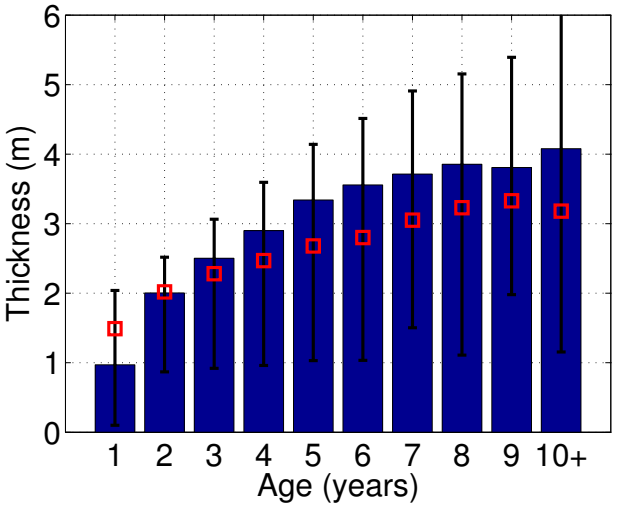

Figure 13: Average March 2003-2006 ice thickness in function of the ice age. 10+ corresponds to ice that is at least 10-years old. The ranges of mean thicknesses over the period are indicated. Also shown is the proxy ice thickness data from Maslanik et al. (2007) for the same period (red squares).

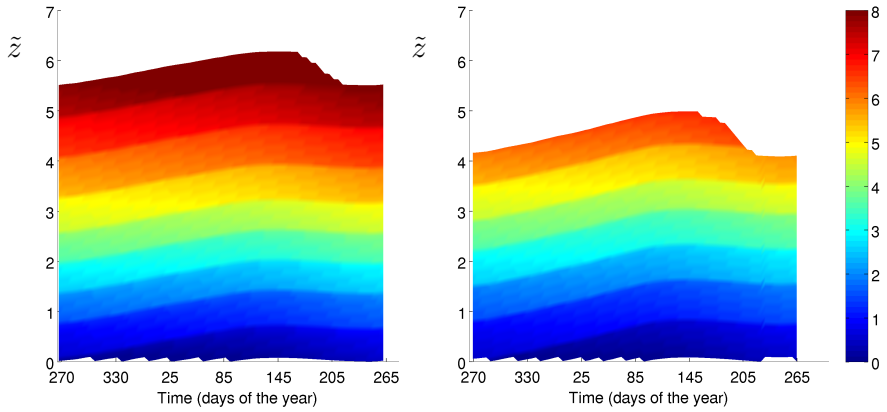

Figure 14: Left: time series of sea ice age (0-8 years) contoured in the $\tilde{z}$ domain. The ice column is situated along Ellesmere Island (near the Canadian Arctic Archipelago, see the red diamond in Fig. 12) for the years 1979-1980, starting at the beginning of the accretion period (days of the year). The sharp variations in colour between two growth seasons are clearly marked, illustrating again the annual layering of the ice column. Right: same, but for the years 2008-2009.

in year classes (first-year, second-year, ...) for climatological analyses. On the left, a first-year ice vertical profile in Laptev Sea is shown. In absence of age discontinuities, quadratic and cubic approximations are in very good agreement with the particles method. Since the Arctic Ocean is the subject of a shift from perennial to seasonal ice (e.g., Maslanik et al., 2007; Nghiem et al., 2007), this is an interesting feature of the method.

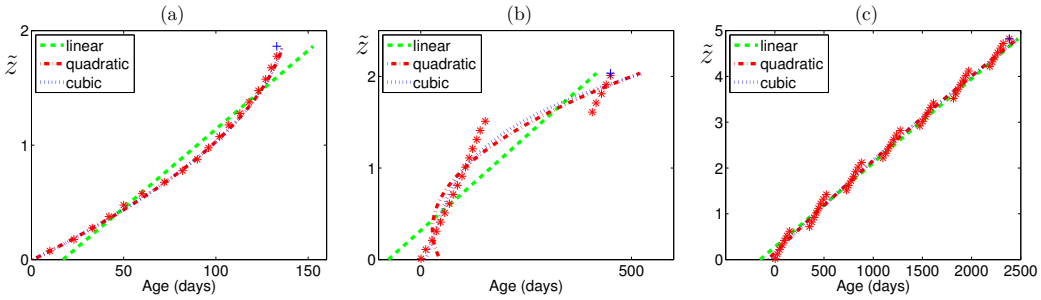

Figure 15: Comparison of vertical age profiles (March 2009) as computed by the Lagrangian particles method (red stars) and the finite element method. The blue cross indicates the ice surface. (a) First-year ice (Laptev Sea, see the red circle in Fig. 12). In absence of age discontinuities, quadratic and cubic approximations are in very good agreement with the particles method. The linear approximation gives a measure of the mean and standard deviation of the age distribution that is as accurate as higher order polynomials. (b) Second-year ice (Beaufort Sea, see the red square in Fig. 12). Differences between the finite element solutions are clearly marked. (c) Multiyear ice (along Ellesmere Island, see the red diamond in Fig. 12).

5 Discussion and conclusions

In this paper, we have introduced a vertically-variable sea ice age, based on the age theory in marine modeling (see, e.g., Delhez et al. (1999) and Deleersnijder et al. (2001)). The age of a sea ice particle is a function of the three spatial coordinates and is interpreted as the time elapsed since its creation. The age is defined here in a geological sense and differs from the ice age derived from satellite data measuring the time elapsed since the whole column of ice has been created. Our developments include the particular case of ice formation at the surface (see the boundary condition (7)).

We have first resolved the sea ice age equation in the framework of an analytical model of sea ice, combining the classical formulation of ice growth by Stefan (1891) and a linearly melting parameterization in time. An analytical solution of this model has been derived. In absence of ice formation at the surface, ice age typically increases upwards and features discontinuities corresponding to the length of the melting periods. Based on the age, the ice column can thus be decomposed in annual growth layers. This annual layering has been reported in past studies (e.g., Cherepanov, 1957; Schwarzacher, 1959). However, these observations of ideal, undeformed multiyear ice are sparse and the stratification is generally less defined in the upper part of the ice experiencing melting and refreezing (Weeks, 2010).

Two numerical methods have been further introduced. The first method involves Lagrangian particles and thereby follows an approach similar to what has been done in, e.g., ice sheet modeling (see Mügge et al. (1999); Rybak and Huybrechts (2003)). This method is adaptive and designed to capture the vertical profile of sea ice age and its discontinuities. Based on the characteristic method, it provides excellent agreement with the analytical solution but is expensive in terms of memory usage (e.g., adding 10 particles to each element is equivalent to adding 10 P_0 tracers on the domain). Increasing the number of particles does not enhance the precison, but merely the "picture" of the vertical age profile that we get. The aim of the second

method is to reproduce the mean and standard deviation of the vertical age profile using as few degrees of freedom as possible. The method uses an ALE spatial discretization and is based on the finite element method. Due to the age discontinuities, the approximations of degree up to three do not accurately represent the vertical distribution in sea ice age, but a linear approximation is sufficient to simulate the mean and standard deviation of the age in reasonable agreement with the analytical solution. In absence of age discontinuities, i.e. for first year ice, a quadratic approximation matches well the results of the Lagrangian approach.

Both methods have been used in a large-scale simulation of the Arctic by accounting for thermodynamic processes only. In this framework, the correlation between ice thickness and ice age as computed by the Lagrangian method is typically high. However, the scatter is significant, and it does not seem feasible to find a unique relationship between ice age and thickness, as pointed out earlier by Hunke and Bitz (2009) and Vancoppenolle et al. (2009) using a different definition. Furthermore, the growth of new ice in leads, transport and piling of ice by deformation may further reduce the age-thickness relationship. In conclusion, our study suggests that the ice age is a good proxy for ice thickness where ice deformation is small or absent. But even in this simplified framework, it is not sufficient to reconstruct ice thickness.

Though the principal contribution to compute the ice age comes from the ice growth/melt rates, the role of dynamics is important in redistributing the ice age profile. The ice transport may change dramatically the atmospheric and oceanic conditions (e.g., multiyear ice exported through Fram Strait) experienced by an ice particle. Piling of ice in regions of strong deformation redistributes the age profile. Taking into account new ice formation in leads should largely increase the ice production and consequently provide a greater volume of young ice. It is therefore expected that the age distribution should significantly deviate from a quasi linear profile, which should reduce the accuracy of the finite element method based on a linear polynomial and should increase the match of higher degree polynomials. The results should also clearly benefit from an oceanic feedback and the oceanic heat advection missing in this model. This should substantially reduce the ice thickness in closer agreement to observations during the last decade.

A perspective of this work is to take the ice dynamics into account and transport the ice age distribution. On the other hand, in future developments, the age must be integrated in the framework of the subgrid-scale ice thickness distribution (ITD, Thorndike et al. (1975)). In both cases, an open issue concerns the "mixing" of age profiles from different categories (ITD) or from different ice columns (transport). Though it should in principle be easy to get a vertically average age content, it sounds much more complex to reconstruct a consistent age profile. Finally, Lagrangian particles might also constitute an interesting and promising method to study the evolution of passive tracers in the ice (e.g., in the biogeochemistry field). Other passive tracers of interest in the ice are δ^{18}O profiles (the ratio between stable oxygen isotopes), which could be easily computed thanks to a Lagrangian sea ice model. Following Pfirman et al. (2004), this would constitute an effective tool to study the evolution of Arctic surface water masses. By computing the sea ice age, the comparison between modeled isotopes profiles and sea ice cores would be easier for the samples presenting an annual stratification.

Acknowledgements

Two anonymous reviewers are gratefully acknowledged for their numerous suggestions and constructive review. We thank Benjamin de Brye, Olivier Gourgue and Jonathan Lambrechts for help on technical topics and implementation issues. The present study was carried out in the framework of the project "Taking up the challenges of multi-scale marine modelling", which is funded by the *Communauté Française de Belgique* under contract ARC 10/15-028 (*Actions de Recherche Concertées*) with the aim of developing and using SLIM (www.climate.be/slim). Eric Deleersnijder is a Research Associate with the Belgian Fund for Scientific Research (F.R.S.-FNRS).

A Coefficients of the system resulting from the spatial ALE discretization

The system resulting from the spatial ALE discretization is the following:

$$\frac{da_i}{dt}(t) = \sum_{j=0}^{p} A_{ij}(t)a_j(t) + \delta_{0i}, \quad i = 0, 1, \ldots, p \tag{59}$$

where $a_i(t)$ are the unknown degrees of freedom and p is the maximum degree of the shape functions. The coefficients of the matrix A can be summerized as follows:

$$A_{ij} = \begin{cases} \sqrt{(2i+1)(2j+1)}((-1)^{i+j}q_b^- + q_s^-) & i < j \\ \sqrt{(2i+1)(2j+1)}((-1)^{i+j+1}q_b^+ - q_s^+) & i > j \\ -(i+1)(q_b^+ + q_s^+) + i(q_b^- + q_s^-) & i = j \end{cases} \tag{60}$$

for $0 \leq i, j \leq p$. For this study, we need the matrices for Legendre polynomials of degree up to three. For a constant polynomial, we have:

$$A = \begin{pmatrix} -q_b^+ - q_s^+ \end{pmatrix}.$$

For constant and linear polynomials, the matrix reads:

$$A = \begin{pmatrix} -q_b^+ - q_s^+ & \sqrt{3}(-q_b^- + q_s^-) \\ \sqrt{3}(q_b^+ - q_s^+) & -2(q_b^+ + q_s^+) + (q_b^- + q_s^-) \end{pmatrix}.$$

With quadratic elements, we have:

$$A = \begin{pmatrix} -q_b^+ - q_s^+ & \sqrt{3}(-q_b^- + q_s^-) & \sqrt{5}(q_b^- + q_s^-) \\ \sqrt{3}(q_b^+ - q_s^+) & -2(q_b^+ + q_s^+) + (q_b^- + q_s^-) & \sqrt{15}(-q_b^- + q_s^-) \\ \sqrt{5}(-q_b^+ - q_s^+) & \sqrt{15}(q_b^+ - q_s^+) & -3(q_b^+ + q_s^+) + 2(q_b^- + q_s^-) \end{pmatrix},$$

while for polynomials of degree up to three:

$$A = \begin{pmatrix} -q_b^+ - q_s^+ & \sqrt{3}(-q_b^- + q_s^-) & \sqrt{5}(q_b^- + q_s^-) & \sqrt{7}(-q_b^- + q_s^-) \\ \sqrt{3}(q_b^+ - q_s^+) & -2(q_b^+ + q_s^+) + (q_b^- + q_s^-) & \sqrt{15}(-q_b^- + q_s^-) & \sqrt{21}(q_b^- + q_s^-) \\ \sqrt{5}(-q_b^+ - q_s^+) & \sqrt{15}(q_b^+ - q_s^+) & -3(q_b^+ + q_s^+) + 2(q_b^- + q_s^-) & \sqrt{35}(-q_b^- + q_s^-) \\ \sqrt{7}(q_b^+ - q_s^+) & \sqrt{21}(-q_b^+ - q_s^+) & \sqrt{35}(q_b^+ - q_s^+) & -4(q_b^+ + q_s^+) + 3(q_b^- + q_s^-) \end{pmatrix}.$$

B Approximation of the analytical solution with piecewise polynomials

In this appendix, we treat the question as to whether it is better to use several piecewise polynomials of low order or one polynomial of higher order. Therefore, we approximate the analytical solution in a leastsquare sense with piecewise polynomials of degree $p = 0$ to $p = 3$ and on an increasing number of elements (see Fig. 16). When no discontinuity is present in the solution (case $N = 1$, where N corresponds to the number of annual growth layers), the expected spatial rate of convergence $p + 1$ is reached for constant and linear approximations (Fig. 17a), while the leastsquare fit is exact to machine precision for higher degree since the solution is of degree 2. For larger values of N (panels b and c), due to the discontinuities in the solution, the order of the method is only $O(h)$ where h is the vertical grid size (i.e., the inverse of the number of elements). In conclusion, increasing the number of elements does not enhance significantly the approximation and a linear polynomial on one element seems to be a good candidate.

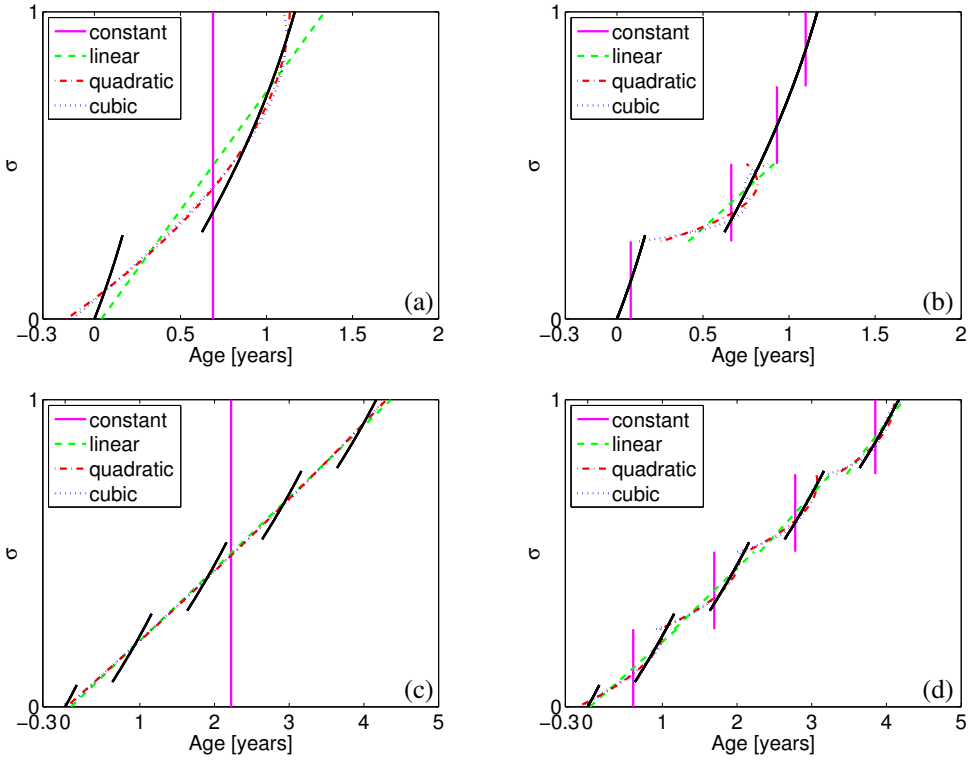

Figure 16: Leastsquare approximation of the analytical solution (solid black line, cf. profiles in Fig. 6) with piecewise polynomials (the degree is mentioned in the legend). Panels (a) and (b): case $N = 2$ with 1 and 4 elements, respectively. (c-d) Same for the case $N = 5$.

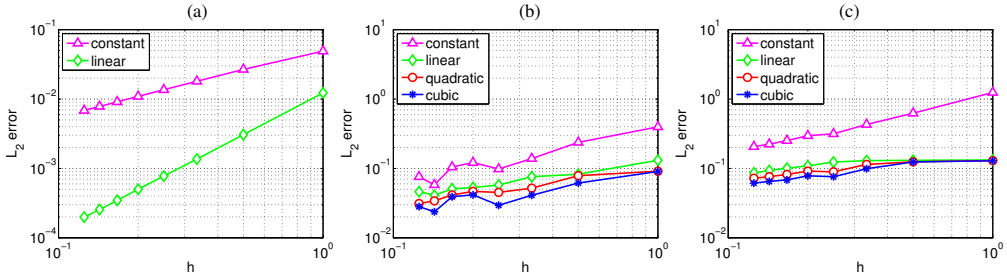

Figure 17: Convergence analysis of the leastsquare approximations (L_2 norm in function of the vertical grid size h). Case $N = 1$ (a), $N = 2$ (b) and $N = 5$ (c). Note the different axes scales.

References

Belchansky, G. I., Douglas, D. C., Platonov, N. G., 2005. Spatial and temporal variations in the age structure of arctic sea ice. Geophys. Res. Lett. 32, L18504.

Berliand, M., Berliand, T., 1952. Determining the net long-wave radiation of the earth with consideration of the effect of cloudiness. Isv. Akad. Nauk SSSR Ser. Geophys. 1 (in Russian).

Berliand, M. E., Strokina, T. G., 1980. Global Distribution of the Total Amount of Clouds. Hydrometeorological Publishing House, Leningrad, Russia. 71 pp (in Russian).

Bourke, R. H., Garrett, R. P., 1987. Sea ice thickness distribution in the arctic ocean. Cold Regions Sci. Technol. 13, 259–280.

Cherepanov, N., 1957. Using the methods of crystal optics for determining the age of drift ice (in russian). Probl. Arktik. 2, 179–184.

Deleersnijder, E., Campin, J.-M., Delhez, E. J. M., 2001. The concept of age in marine modelling i. theory and preliminary model results. Journal of Marine Systems 28, 229–267.

Delhez, E., Campin, J.-M., Hirst, A., Deleersnijder, E., 1999. Toward a general theory of the age in ocean modelling. Ocean Modelling 1, 17–27.

Donea, J., Huerta, A., Ponthot, J.-P., Rodrìguez-Ferran, A., 2004. Encyclopedia of computational mechanics - Volume 1. Wiley, Ch. 14, pp. 413–437.

Eicken, H., Grenfell, T. C., Perovich, D. K., Richter-Menge, J. A., Frey, K., 2004. Hydraulic controls of summer arctic pack ice albedo. J. Geophys. Res. 109, C08007.

Fichefet, T., Goosse, H., Maqueda, M. A. M., 1998. Ocean Modeling and Parameterization. Vol. C516 of NATO ASI Series. Kluwer Academic Publisher, Dordrecht, Ch. On the large-scale modeling of sea ice–ocean interactions, pp. 399–422.

Fowler, C., Emery, W. J., Maslanik, J., 2004. Satellite-derived evolution of arctic sea ice age: October 1978 to march 2003. IEEE Geosci. Remote Sens. Lett. 1, 71–74.

Goosse, H., 1997. Modelling the large scale behaviour of the coupled ocean–sea-ice system. Ph.D. thesis, Université catholique de Louvain, Louvain-la-Neuve, Belgium, 231 pp.

Haas, C., Hendricks, S., Eicken, H., Herber, A., 2010. Synoptic airborne thickness surveys reveal state of arctic sea ice cover. Geophys. Res. Lett. 37, L09501.

Harder, M., 1997. Roughness, age and drift trajectories of sea ice in large-scale simulations and their use in model verifications. Ann. Glaciol. 25, 237–240.

Hunke, E. C., Bitz, C. M., 2009. Age characteristics in a multidecadal arctic sea ice simulation. J. Geophys. Res. 114, C08013.

Kovacs, A., 1997. Estimating the full-scale flexural and compressive strength of first-year sea ice. J Geophys. Res. 102, 8681–8689.

Lietaer, O., Fichefet, T., Legat, V., 2008. The effects of resolving the Canadian Arctic Archipelago in a finite element sea ice model. Ocean Modelling 24, 140–152.

Maslanik, J. A., Fowler, C., Stroeve, J., Drobot, S., Zwally, J., Yi, D., Emery, W., 2007. A younger, thinner arctic ice cover: Increased potential for rapid, extensive sea-ice loss. Geophys. Res. Lett. 34, L24501.

Mügge, B., Savvin, A., Calov, R., Greve, R., 1999. Numerical age computation of the antarctic ice sheet for dating deep ice cores. Springer-Verlag, Ch. Advances in Cold-Region Thermal Engineering and Sciences, pp. 307–318.

Nakawo, M., Sinha, N. K., 1981. Growth rate and salinity profile of first-year sea ice in the high arctic. J. Glaciol. 27, 315–331.

Nghiem, S. V., Rigor, I. G., Perovich, D. K., Clemente-Colon, P., Weatherly, J. W., Neumann, G., 2007. Rapid reduction of arctic perennial sea ice. Geophys. Res. Lett. 34, L19504.

Pfirman, S., Haxby, W., Eicken, H., Jeffries, M., Bauch, D., 2004. Drifting arctic sea ice archives changes in ocean surface conditions. Geophys. Res. Lett. 31, L19401.

Phillips, N. A., 1957. A coordinate system having some special advantages for numerical forecasting. Journal of Meteorology 14, 184–185.

Rigor, I. G., Wallace, J. M., 2004. Variations in the age of arctic sea-ice and summer sea-ice extent. Geophys. Res. Lett. 31, L09401.

Rothrock, D. A., Percival, D. B., Wensnahan, M., 2008. The decline in arctic sea-ice thickness: Separating the spatial, annual, and interannual variability in a quarter century of submarine data. J. Geophys. Res. 113, C05003.

Rybak, O., Huybrechts, P., 2003. A comparison of eulerian and lagrangian methods for dating in numerical ice-sheet models. Annals of Glaciology 37, 150–158.

Schwarzacher, W., 1959. Pack-ice studies in the arctic ocean. J. Geophys. Res. 64, 2357–2367.

Semtner, A. J., 1976. A model for the thermodynamic growth of sea ice in numerical investigations of climate. J. Phys. Oceanogr. 6, 379–389.

Steele, M., Morley, R., Ermold, W., 2001. Phc: a global ocean hydrography with a high quality arctic ocean. J. Climate 14, 2079–2087.

Stefan, J., 1891. Über die theorie des eisbildung, insbesondere über eisbildung im polarmeere. Annalen der Physik 42 (3rd Ser.), 269–286.

Thorndike, A. S., Rothrock, D. A., Maykut, G. A., Colony, R., 1975. The thickness distribution of sea ice. J. Geophys. Res. 80, 4501–4513.

Timco, G. W., Frederking, R. M. W., 1990. Compressive strength of sea ice sheets. Cold Regions Science and Technology 17, 227–240.

Trenberth, K. E., Olson, J. G., Large, W. G., 1989. A global ocean wind stress climatology based on ecmwf analyses. Tech. Rep. NCAR/TN-338+STR, National Center for Atmos. Res., Boulder, Colorado, 93 pp.

Vancoppenolle, M., Fichefet, T., Goosse, H., Bouillon, S., Madec, G., Morales Maqueda, M., 2009. Simulating the mass balance and salinity of arctic and antarctic sea ice. 1. model description and validation. Ocean Modelling 27, 33–53.

Walsh, J. E., Zwally, H. J., 1990. Multiyear sea ice in the arctic: Model- and satellite-derived. J. Geophys. Res. 95(C7), 11613–11628.

Weeks, W. F., 2010. On Sea Ice. University of Alaska Press, Fairbanks, Alaska. 664 pp.

Zillmann, J., 1972. A study of some aspects of the radiation and the heat budgets of the southern hemisphere oceans. In: Meteorol. Stud. Vol. 26. Bur. Meteorol. Dep. of the Interior, Canberra, Australia, p. 562.